Summer Intership Report

Dong Chengyu

July 2, 2017

Abstract

Nuclear ring type is possible to be indicated by the enclosed mass. The existence of one explicit criterion of enclosed mass to determine the ring type is denied but the grey region denoted by a bunch of boundaries may be an alternative choice. Double ring appears frequently in our numerical simulation despite the absence in the real nature. A possible explanation has been introduced to interpret this phenomenon qualitatively.

1 Model a barred galaxy

1.1 Introduction

Nuclear rings are generally considered as the result of nonlinear interactions of gas under a specific bar potential. Induced by the bar torque, a ring-like structure grows close to the centre as gas flows inward along the dust lanes residing in the leading side of the bar. Numerous works have been done to explore the relations between the bar potential and the nuclear ring by simulations. To model a barred galaxy, apparently we need at least a gas disk, a stellar bar and a central galactic bulge; sometimes a central black hole will also be introduced to the model. In order to simplify the model, we assume that the gas is isothermal hence we can get rid of temperature, which is usually a complicated parameter; and we also neglect the gas self-gravity and star formation that occurs in high-density nuclear rings. The gas self-gravity has little influence on the overall structure according to the previous work (Kim et al.2012) and the star formation's effect has yet to be learned.

In our model, the bar is assumed to rotate rigidly about the galaxy centre with a fixed pattern speed Ω_b . The equations of ideal hydrodynamics in a frame co-rotating with the bar are

$$(\frac{\partial}{\partial t} + \boldsymbol{u} \cdot \nabla)\Sigma = -\Sigma \nabla \cdot \boldsymbol{u}, \tag{1}$$

Figure 1: An example of nuclear ring.

$$(\frac{\partial}{\partial t} + \boldsymbol{u} \cdot \nabla)\boldsymbol{u} = -c_s^2 \frac{\nabla \Sigma}{\Sigma} - \nabla \Phi_{ext} + \Omega_b^2 \boldsymbol{R} - 2\boldsymbol{\Omega_b} \times \boldsymbol{u}. \tag{2}$$

Here Σ and $\boldsymbol{u}$ denote the gas surface density and velocity respectively. Equation (1) is the continuity equation and Equation (2) is the momentum equation in co-rotating cylindrical polar coordinates.

1.2 The galaxy model

Here we briefly summarise our numerical models. Potential comprised of four components maintains the rotation of the gas disk. First are the two axisymmetric components. The disk we introduce here is a Kuzmin-Toomre stellar disk (Kuzmin 1956; Toomre 1963) of surface density

$$\sigma(r) = \frac{V_0^2}{2\pi G r}(1 + \frac{r^2}{r_0^2})^{-1.5}. \tag{3}$$

It's a infinitesimally thin 2D gaseous disk containing two parameters V_0 and r_0 which set the scales for the velocities and radii respectively. They will be given fixed values, i.e. $260\,\mathrm{km} \cdot \mathrm{s}^{-1}$ and $14.1\,\mathrm{kpc}$ respectively in our simulations.

To represent the galaxy bulge, we take a modified Hubble profile of volume density

$$\rho(r) = \rho_b(1 + \frac{r^2}{r_b^2})^{-1.5}, \tag{4}$$

where ρ_b and r_b represent the bulge central density and scale length respectively. A high central density ρ_b means high central concentration, which denotes a more compact galaxy.

Finally, to describe the galaxy bar, we use an n=1 inhomogeneous Ferrers ellipsoid with volume density

$$\rho = \begin{cases} \rho_{bar}(1-g^2)^n & \text{for g} < 1, \\ 0 & \text{elsewhere,} \end{cases} \tag{5}$$

$$g^2 = y^2/a^2 + (x^2+z^2)/b^2. \tag{6}$$

The bar central density ρ_{bar}, major axis a and minor axis b of the bar are fixed at $4.47 \times 10^8\, M_\odot\, kpc^{-3}$, 5, and $2\, kpc$, respectively. This gives a bar axis ratio of 2.5 and a bar mass of $1.5 \times 10^{10}\, M_\odot$. The shape and mass of the bar are fixed for all the models. In our simulations, we start with an axis-symmetrized bar and the bar mass is linearly ramped up to its final maximum (Athanassoula 1992b) to avoid transients.

To make it more realistic, we add a black hole in the centre with density

$$\rho(r) = \frac{3M_{BH}}{4\pi r_s^3}(1+\frac{r^2}{r_s^2})^{-2.5}, \tag{7}$$

where M_{BH} is the total mass of the black hole and r_s is the softening radius. The two parameters will be given fixed values as $M_{BH} = 10^7\, M_\odot$ and $1pc$ respectively. With $M_{BH} \ll M_{disk}, M_{bulge}, M_{bar}$, the BH will only exert its effect in the very central regions ($R \lesssim 0.5\, kpc$).

All these models put together denote a reasonable rotation curve, which is plotted in Figure 2.

1.3 Our main concern

According to previous works (Mazzuca 2011; Athanasoula 1992b), the size, shape and position of nuclear ring may all relate to the compactness or central concentration of the galaxy. Particularly, in the latest work (LiZhi et al. 2015), it is argued that the enclosed mass of bulge may have a substantial impact on the nuclear ring type (x_1-type or x_2-type). However, a more explicit criterion is absent. Moreover, whether or not this criterion can be applied to a realistic galaxy which may have a bulge of totally different density profile from the one used now remains an unknown question. We are dedicated to work this out for that if we can relate the enclosed mass within a specific radius to the nuclear ring's type, given an observation result of the mass distribution of a realistic galaxy, we are able to directly come up with the existence of the nuclear ring because of the absence of x_1 types ring in the real galaxies and vice visa.

We hence adjust the parameters ρ_b and r_b of the bulge model with other parameters fixed to generate bulge enclosed mass percentages and pay close attention to the nuclear ring type to find out some particular criterions that reveal the mere effects of the bulge enclosed mass by quantities of simulations. Meanwhile, several models with different density profiles will also be introduced to testify the applicability of these criterions.

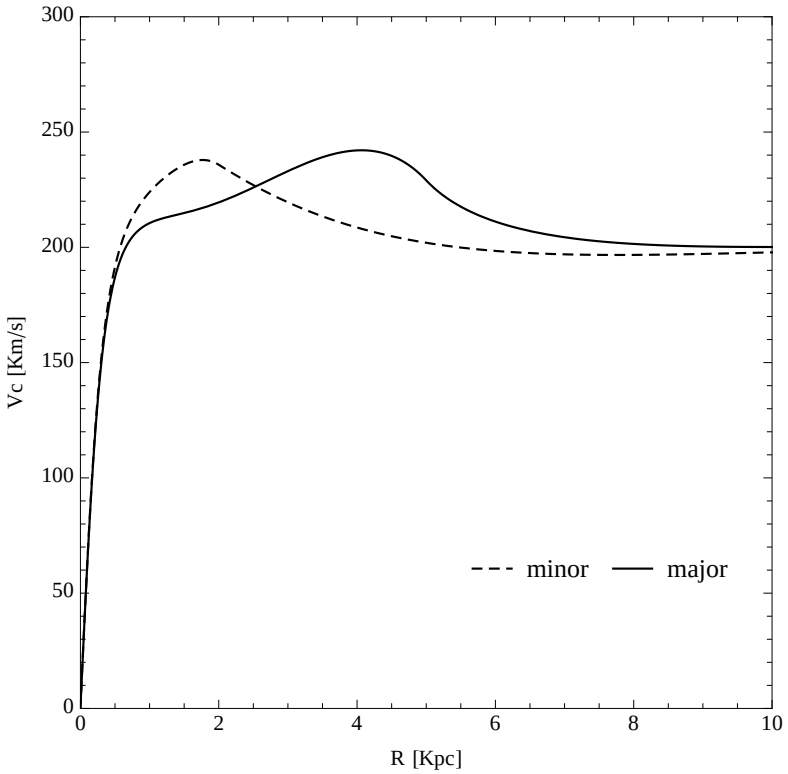

Figure 2: Rotation velocity of our model galaxy. The solid and dashed line are for along the bar major and minor axes, respectively. Here the innermost BH's contribution is neglected for simplification.

2 Hubble profile bulge and the boundaries

2.1 Parameters and properties of Hubble profile

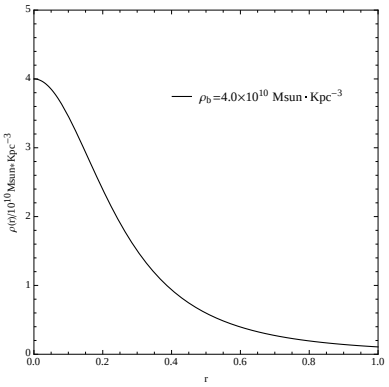

Figure 3: Typical density distribution of Hubble profile

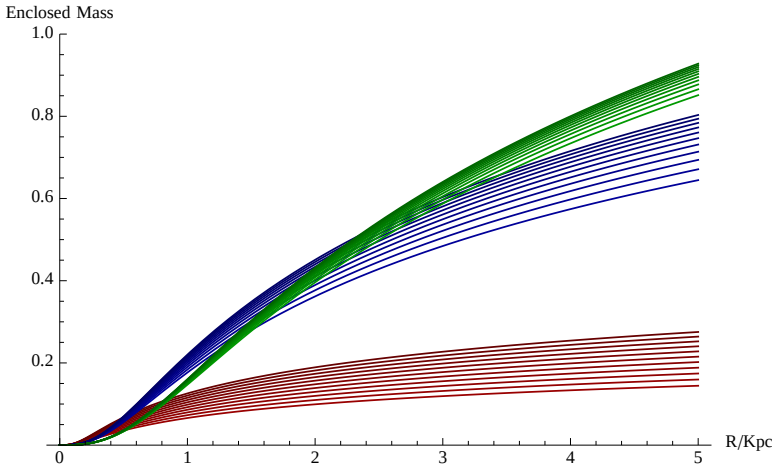

Figure 4: Groups of bulge enclosed mass curves. The green, blue and red lines correspond to r_b equals 0.8, 0.5 and $0.2\,\mathrm{Kpc}$ respectively. The darker ones in each group are of higher ρ_b.

Figure 3 shows a typical density distribution of Hubble profile, which we use to model the bulge. Apparently, Hubble profile has a finite density in the very centre, and gradually decreases when moving outwards. Since we aim to explore the effects of the

Figure 5: Enclosed mass percentage versus different r_b values. The curves are not monotone apparently. Gradually darker ones correspond to enclosed radii ranging from 0.1 to $1.0\,\mathrm{Kpc}$. Here ρ_b is fixed to $2.35 \times 10^{10}\, M_\odot \cdot \mathrm{Kpc}^{-3}$

enclosed mass, we have to adjust the parameters of the profile. Figure 4 depicts different groups of enclosed mass percentage curves with different r_b, while in each group ρ_b varies continuously.

Here enclosed mass percentage we simply defined is the percentage of bulge mass within radius r over the total mass within $5\,Kpc$ (The bar's semi-major axis) namely

$$Enclosed\,mass\,percentage = \frac{M_{bulge}(r)}{M_{total}(5)} \times 100\%.$$

It is clear on the plot that for each specific value of r_b, as ρ_b increases continuously (The darker, the higher value), the curves are gradually lift up. Since the curves in one group change in succession and sweep over a region, there must be a turn-over boundary that separate x_2-type nuclear rings to x_1-type ones, which means as for this specific value of r_b, if ρ_b is lower than the boundary value, then x_2-type nuclear rings can not form. Hence if we test several groups with several different r_b values, a number of turn-over boundaries can be found out, with which we can seek out the correlation between bulge enclosed mass and the substantial variation of nuclear ring types.

There's another reason why we use r_b tag different groups and ρ_b as the variable in each group. As Figure 5 depicts, while r_b varies from $0.1\,\mathrm{Kpc}$ to $1.0\,\mathrm{Kpc}$, the enclosed mass percentage increases and then decreases, which means higher value of r_b may not correspond to higher enclosed mass percentage. Therefore if we exchange the roles of the two parameters, some unexpected faults may occur.

2.2 Simulation results

Figure 6 shows the simulation results for all kinds of parameters. Parameter r_b gradually increases from upper to bottom, while parameter ρ_b gradually increases from left to right. The boundaries mentioned above have been highlighted in red boxes. It is obvious that a galaxy model with high value of r_b turns from x_1-type nuclear ring to x_2-type one at a relative low value of ρ_b. In the addition, there are a few interesting findings among these numbers of simulation results like the double ring, which we will figure it out later in detail.

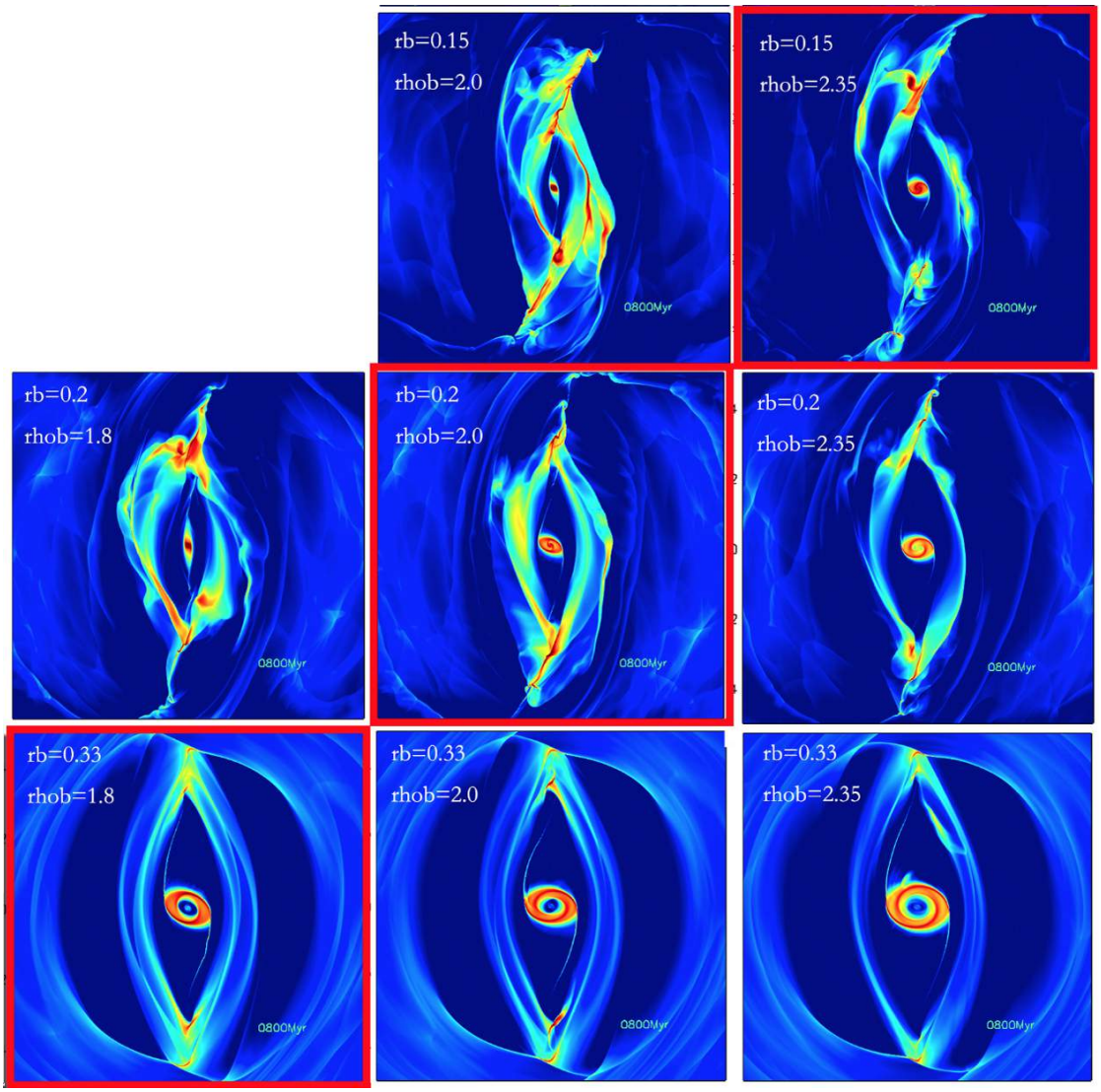

Figure 6: A part of the simulation results of Hubble profile (The whole will be attached). Parameter r_b gradually increases from upper to bottom, while parameter ρ_b gradually increases from left to right. The contour plots in red boxes denote the boundary between x_1 and x_2 ring types.

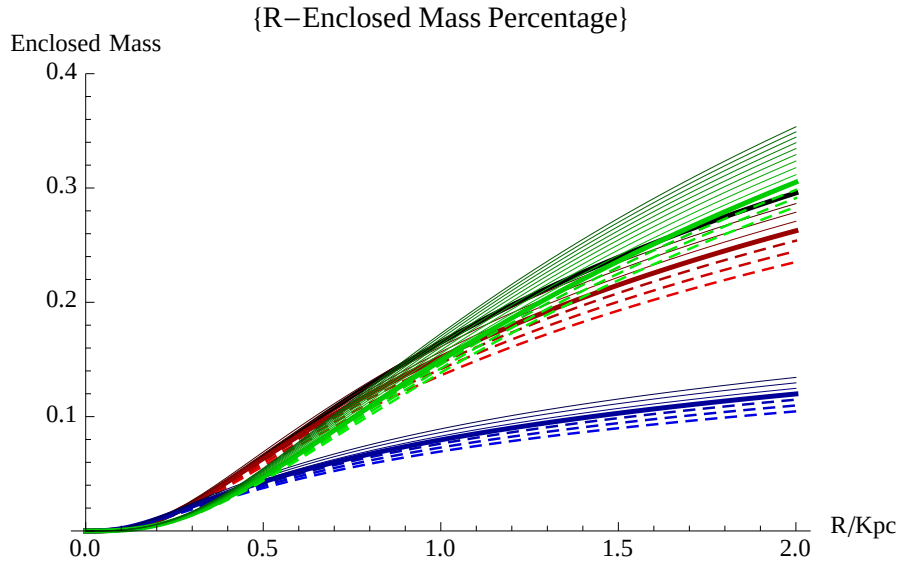

Figure 7: Boundaries for different r_b groups. The green, red and blue lines correspond to r_b equals 0.5, 0.33, $0.2\,\mathrm{Kpc}$ respectively. The solid line separates x_1 and x_2 ring types in each group while the black thick line correspond to the boundary in total-mass-constant condition.

2.3 The boundaries and the grey region

Here we present the simulation results on the radius-enclosed mass percentage plot. In Figure 7, the dashed curves correspond to x_1-type rings, while the thick curve in each group depicts the boundary as mentioned above. The black thick curve depicts the boundary in the group that the total mass within $10\,\mathrm{Kpc}$ (the outmost radius in the simulation) remains constant (This group is neglected in the figure for simplicity.). If there's one explicit criterion, that right at this position this specific enclosed mass value can tell the ring type, then all the boundaries on the plot must intersect at just one point. Apparently, the boundaries intersects almost everywhere, so we are unable to give an explicit enclosed mass criterion to decide the ring type.

However, a "No" answer is not equal to that there is "not" any relation between enclosed mass percentage and the nuclear ring type. If we re-draw the boundaries on a log-log plot (Figure 8), it's clear that all the intersections mainly resides in a small region that ranges from $0.2\,\mathrm{Kpc}$ to $1.0\,\mathrm{Kpc}$ approximately, which reveals that the very inner region of a galaxy is what really counts. And as far as some moderate values of bulge scale length are concerned (less than $0.5\,\mathrm{Kpc}$), an enclosed mass percentage of 2.0% at $0.25\,\mathrm{Kpc}$ tends an estimate to decide the ring types.

Furthermore, whereas the region below each boundary is certain to determine a x_1-

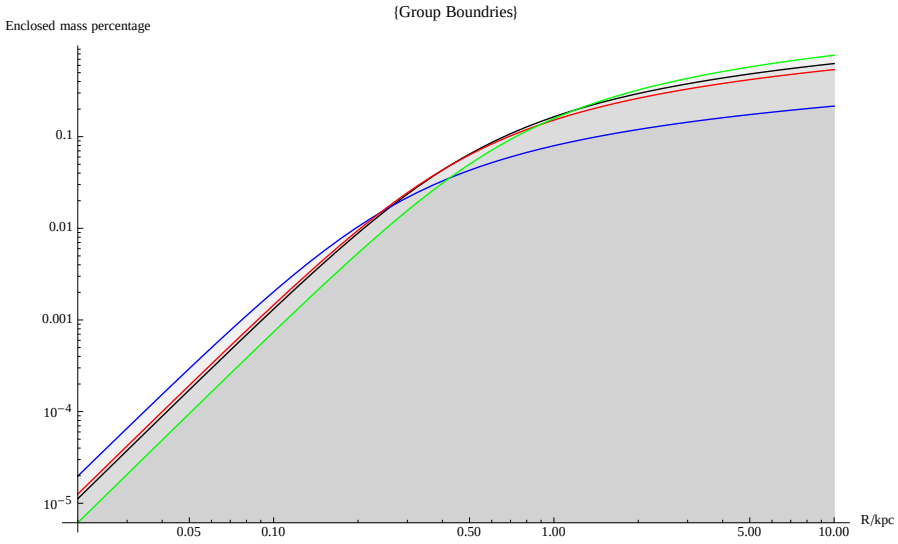

Figure 8: Same as above, but log-log plots.

type ring, we might as well put all these regions together to make up a large grey region as shown in Figure 8. As to Hubble profile we mentioned now, if an enclosed mass curve is able to generate x_2-type ring, it has to reside above any of the boundaries, then some parts of this curve surely have exceeded the grey region. Hence if a curve is totally embedded in the grey region, it is impossible to generate x_2-type ring. So far, the grey region seems a graveyard, which definitely separates the two kinds of ring types. Moreover, given a bold hypothesis that the grey region can be applied to any bulge profile, one can straightforwardly decide whether or not there can form $x_2$type nuclear ring according to the observation data of bulge mass distribution. It plays exact the same role as the one-percentage-at-one-position criterion as mentioned above.

To testify this splendid idea, we introduce another bulge profile.

3 Hernquist profile

Here we introduce another bulge profile namely Hernquist profile:

$$\rho(r) = \frac{M}{2\pi}\frac{r_b}{r}\frac{1}{(r+r_b)^3}, \tag{8}$$

where r_b represents a characteristic length scale of the bulge and M is the total mass.

Figure 9 shows the density distribution of a Hernquist profile. Due to the infinite density in the center of the bulge, the angular frequency is extremely steep in the centre (Figure 10) and there is only one ILR ($\Omega - \kappa/2 = \Omega_b$) for a typical pattern speed

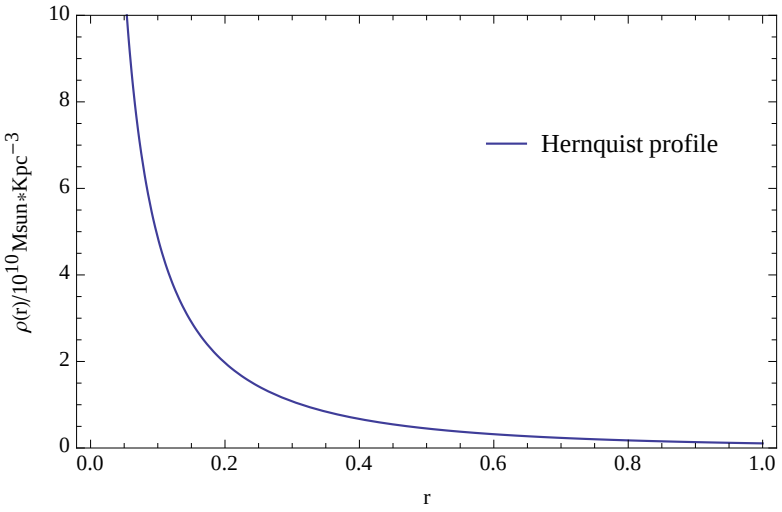

Figure 9: A typical density distribution of Hernquist profile.

$33\,\mathrm{Km}\cdot\mathrm{s}^{-1}\cdot\mathrm{Kpc}^{-1}$, which means the x_2 type periodic orbits probably have no inner confinement and extend straight to the very centre.

Regardless of the infeasibility, we still plot the enclosed mass curves of the Hernquist profile together with the grey region as mentioned (Figure 12). It's obvious that the curve of the Hernquist profile hang high over the grey region in the centre, though we have chosen very low bulge mass values ($0.5 < M_{\mathrm{within}\,10\,\mathrm{Kpc}} < 2.5\,10^{10}\,M_{\odot}$). Hence it is demonstrated here again that the inner region of the bulge has great significance.

4 Plummer profile

Now that the Hernquist profile fails as a touchstone, we have to find another bulge profile. Plummer profile appears in previous work (Kim et al. 2012b) to model the central black hole. It is a power-law density model similar to Hubble profile with volume density

$$\rho(r) = \rho_b(1 + \frac{r^2}{r_b^2})^{-2.5} \tag{9}$$

where ρ_b is the central density and r_b the scale length. Figure 13 shows a contrast between Plummer profile and Hubble profile, whose parameters are set the same values. The two's density distribution seems quite similar despite the compactness. The simulation results seems similar as well if given appropriate values as Figure 14 shows. Therefore, we did the same thing as what have been done to Hubble profile to find the boundaries and draw them together with the grey region (Figure 15). The red, purple

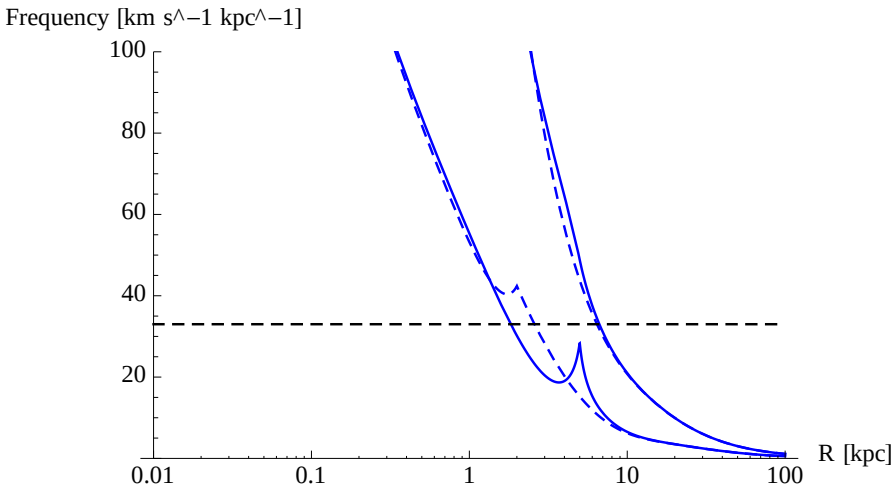

Figure 10: Angular frequency curves for Hernquist profile. The left one denotes $\Omega - \kappa/2$ while the right one denotes Ω. The dashed and solid line correspond to the angular frequency along bar minor and major axis respectively. The horizontal black dashed line denotes bar pattern speed ($\Omega_b = 33\,\mathrm{Km}\cdot\mathrm{s}^{-1}\cdot\mathrm{Kpc}^{-1}$). Intersections between the left curves and the black line represent ILR.

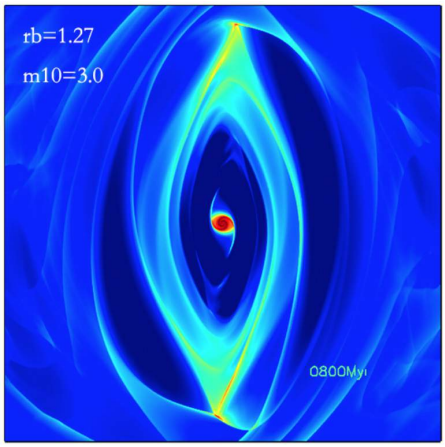

Figure 11: A typical simulation result for Hernquist profile bulge with very low mass. Despite the extremely small size, the nuclear ring still appear as a x_2-type.

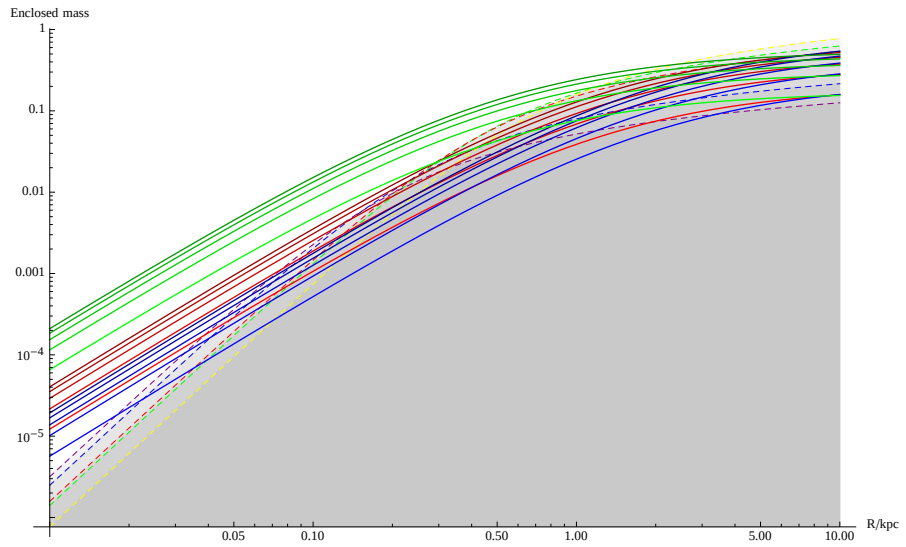

Figure 12: The enclosed mass curves of the Hernquist profile together with the grey region depicted by Hubble profile. The blue, red and green curves with Hernquist profile correspond to r_b equals 2.0, 1.2, $0.5\,\mathrm{Kpc}$ respectively, while ρ_b in each group ranges from 0.5 to $2.5 \times 10^{10}\,M_\odot \cdot \mathrm{Kpc}^{-3}$ from lighter curves to darker ones. The Dashed curves correspond to Boundaries in Hubble profile as given above. Though given an extremely low ρ_b value, the curves for Hernquist profile still extend quite a lot beyond the boundaries defined by Hubble profile in the inner region.

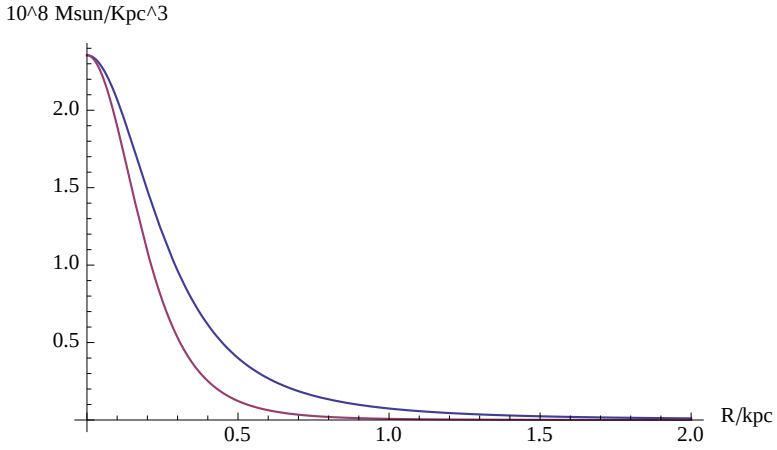

Figure 13: Contrast between the density distribution of Hubble and Plummer profile. The parameters of Both are given the corresponding same value.

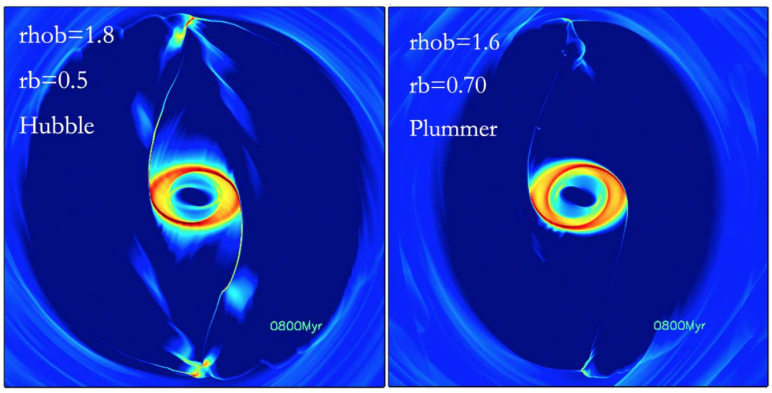

Figure 14: Contrast between typical simulation results of Hubble and Plummer profile.

and orange curves correspond to $r_b = 0.5$, $r_b = 0.7$ and $r_b = 1.0$ respectively, while the dashed and solid ones relate to x_1 and x_2-type rings respectively. ρ_b of dashed and solid curves for red, purple and orange ones list in sequence: 1.4, 1.6, 1.2, 1.4, 1.0, $1.2 \times 10^{10}\, M_\odot \cdot \mathrm{Kpc}^{-3}$.

In general, the pre-defined grey region and the boundaries denoted by Plummer profile are in accord with each other, considering that we only take a few groups for examples. In addition, the boundaries of Plummer profile mainly intersect ranging from $0.5\,\mathrm{Kpc}$ to $1.0\,\mathrm{Kpc}$, almost the same as that of Hubble profile, which again emphasis the indispensable significance of this region.

However, the slight deviation of the Plummer profile should not be neglected. If the grey region could be put into practice, the final results of any profile or even any kinds of mass distribution should be precisely identical for that any density distribution which falls into the "the fuzzy region" amid different boundaries presents a paradox against our argument. We propose that the deviation between the two profiles so far comes from the deficient expression of the enclosed mass percentage, which results from our ignorance to the real mechanism on how the enclosed mass affects the ring formation. To continue the work, on one hand we need more profiles and all kinds of peculiar density distribution to test and conclude their common properties about the boundaries. More importantly, we require deeper exploration about the angular momentum transmission and periodic orbits which is the key to understand the nuclear ring.

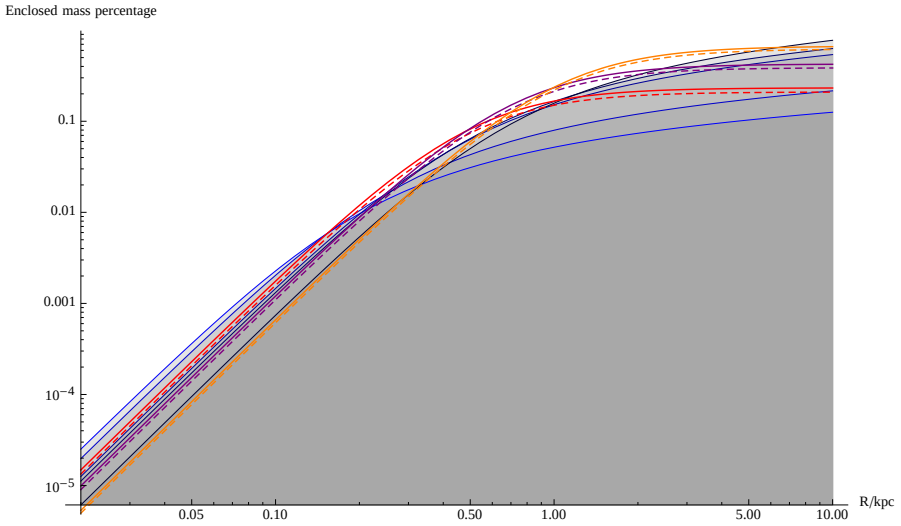

Figure 15: The enclosed mass curves of the Plummer profile together with the grey region depicted by Hubble profile. The red, purple and orange curves with Plummer profile correspond to $r_b = 0.5$, $r_b = 0.7$ and $r_b = 1.0$ respectively, while the dashed and solid ones represent x_1 and x_2-type rings respectively. The blue curves depict the boundaries defined by Hubble profile same as above. ρ_b of dashed and solid curves for red, purple and orange ones list in sequence: 1.4, 1.6, 1.2, 1.4, 1.0, $1.2 \times 10^{10}\, M_\odot \cdot \mathrm{Kpc}^{-3}$.

5 Sensitive to the index?

Up to now we have introduced two profiles into the simulation, whose density fit a general expression, namely

$$\rho(r) = A \times \rho_b (1 + \frac{r^2}{r_b^2})^{-\alpha}. \tag{10}$$

The most simple and direct way to test the effectiveness of the grey region is to compare the shift of these regions due to the different indices in the expression. If the shift or deviation be amplified as index varies, the grey region certainly makes no sense. Firstly and obviously, A has no effect on the position and shape of the region. α is a knotty problem. Now that we have the result of $\alpha = 1.5, 2.5$, the next is to use an even bigger index like 5. No matter it is realistic or not, the result may contribute to the judgement.

6 Conclusion

Nuclear rings play an important role in the evolution of barred galaxies. Since it is believed that the nuclear ring forms where the centripetal and centrifugal force achieve a balance and the centripetal force is closely related to the enclosed mass, we propose that the enclosed mass may become a useable and simple indicator to estimate the nuclear ring type. Through numerous simulations and theoretical analysis, we deny the existence of one explicit criterion to determine the ring type, but a bunch of boundaries and thus the grey region may be useful to do the same work alternatively. However, the feasibility of this idea is yet to be examined and more internal mechanisms and theoretical explanations are required.

7 The double ring

7.1 Simulation results

In our numerous simulations, gas in several groups exhibits some unusual and notable features. Given appropriate parameters, a clump of gas is inclined to lie slightly inside the nuclear ring with no evident communication to the surroundings and roughly develops into x_1-type ring. Now that two rings both form in the very centre, we might as well call it the double ring phenomenon. Figure 16 shows one typical example of these results.

It ought to be noticed that the double ring is not a transient and accidental phenomenon. By not be transient I mean if given appropriate parameters, the inner ring

Figure 16: An example of double ring. The parameters are as follows: $\rho_b = 1.8 \times 10^{10}\, M_\odot \cdot \mathrm{Kpc}^{-3}$, $r_b = 0.6\,\mathrm{Kpc}$

emerges, develops and is able to exist stably up to the end of this simulation, despite that in most cases the inner ring is indeed around for a while and then disappear. Meanwhile, by not be accidental I mean that the double ring phenomenon is not simply noticeable when the parameters given specific values and interceptive with other values close to it. It is a successive phenomenon as the parameters vary in continuous values, which can be easily figured out in Figure 17 with the results of four similar groups of parameters.

Figure 17: Simulation results with four similar groups of parameters. r_b is fixed to $0.6\,\mathrm{Kpc}$ while ρ_b increase from 1.5 to 1.8 with $0.1 \times 10^{10}\,M_\odot \cdot \mathrm{Kpc}^{-3}$ interval. As ρ_b increases, the nuclear spiral arms in the upper-left figure gradually develop apart from the nuclear ring and end in an independent clump of gas in the bottom-right one.

7.2 Possible explanation

Here we give a possible explanation to the double ring phenomenon, which is mainly based on qualitative analysis.

Before we discuss the origin of double ring, there are two inferences drawn from the previous work which need to be acknowledged.

First we need to admit that there must be some primal gas round the centre able to survive the exclusion of the bar torque. The density wave stirred by the external potential plays an important role in the early evolution of the gas. The wave arms in the centre, roughly on $0.2\mathrm{Kpc}$ (Figure 18, left), survive considerably long (Figure 18, right) since the bar torque exerted over the gas is obviously low in the centre (Figure 18, middle). This clump of gas residual dominated by the early density wave, with relatively low angular momentum compared to the nuclear ring which origins in the outer region and later falls inside in the shock, is certain to interact with nuclear ring after the density wave gradually dissipates.

Therefore here comes our second inference that there must be strong interaction between the primal gas residual and the nuclear ring considering their neighbourhood. By adding a extremely massive black hole ($4 \times 10^8\, M_\odot$), more central gas survives due to the effective centripetal force exerted by the black hole, and we can almost notice a huge gas disk around the centre (Figure 19). Under this circumstance, the nuclear ring clearly shrinks long after the bar finishes growing as Figure 20 shows that either the peak of the density cut along the bar major axis or minor one moves inwards from $500\,\mathrm{Myr}$ to $900\,\mathrm{Myr}$. Since the bar potential finishes growing around $300\,\mathrm{Myr}$ and the whole potential exerted on the gas is time constant, the nuclear ring should have gradually stabilised. Thus this peculiar shrinking behaviour tends to reveal the close communication between the gas residual disk and the nuclear ring in the way that the nuclear ring absorbs the low angular momentum holden by the primal gas and moves inwards as its average angular momentum decreases.

With the two inferences mentioned above, we are able to figure out a brief scenario concerning the formation of the inner ring. On the beginning, the gas round the centre led by the primal density wave survives the relatively low bar torque and inherited its born low angular momentum, which is a general process in the simulation. However, from now on, with the dissipation of the density wave and the interference of the nuclear ring, the fate of this clump of gas develops in all roads.

In one extreme case, that the nuclear ring is so small that the gas residual interacts with it vigorously (Figure 21a), the primal gas lacking enough space to evolve independently, has to act as the channel between the nuclear ring and the very centre, namely the nuclear spiral arm (Figure 21b), and later merge with the ring (Figure 21c).

In another extreme case, that the nuclear ring is considerably large, basically after the dissipation of density wave, there is no evident communication between the nuclear ring and the primal gas residual (Figure 22a). Hence the central gas residual becomes

Figure 18: Density wave and primal gas residual. The left and right is the snapshot of one simulation on 100 and $200\,\mathrm{Myr}$ respectively. The middle is the bar torque namely $|r \times F|$. The dashed white line shows the approximate position of the primal gas residual dominated by early density wave and forced by low bar torque.

Figure 19: The simulation result with a massive black hole whose mass is up to $4 \times 10^8\, M_\odot$ on $600\,\mathrm{Myr}$. A huge gas disk exists inside the nuclear ring. The parameters are as follow: $r_b = 0.6\,\mathrm{Kpc}$; $\rho_b = 1.8 \times 10^{10}\, M_\odot \cdot \mathrm{Kpc}^{-3}$.

(a) On $500\,\mathrm{Myr}$ (b) On $900\,\mathrm{Myr}$

Figure 20: Density cut in the massive black hole model mentioned above along the bar major (red and solid) and minor (blue and dashed) axes. The density peak namely the approximate location of the nuclear ring on $900\,\mathrm{Myr}$ obviously moves further inwards compared to its previous location on $500\,\mathrm{Myr}$.

isolated to evolve independently. In the addition, because of the rather large size of the nuclear ring, the gas residual has just the appropriate periodic orbit fairly close to the nuclear ring to dwell on. Finally, because of the early communication with the nuclear ring, the gas residual with a slightly higher angular momentum compared to the original angular momentum at this location, is inclined to run on x_1-type orbit which turns out an inner ring extending along the bar major axis (Figure 22b). Another possible explanation for the x_1-type ring is that at such a central location, there are not likely to be any x_2-type orbits.

Apart from the two extreme cases, we surely have quite a few neutral cases, which implies in one simulation the strong interaction with the nuclear ring and the inner isolated ring both exist, but transiently. Figure 23 shows this kind of process in detail. On $400\,\mathrm{Myr}$, the density wave nearly dissipates and the gas residual becomes isolated. On $570\,\mathrm{Myr}$, the gas resides on x_1-type periodic orbit and forms the inner ring extending along the bar major axis. So far, it is similar to the large nuclear ring case. Nevertheless, on $800\,\mathrm{Myr}$, the inner ring precesses and leans away from the bar major axis, which leads to the close communication with the nuclear ring. Later to the end, the inner ring has no way to precess back and become a part of the nuclear ring on $1000\,\mathrm{Myr}$. It is obvious that two factors lead to this kind of neutral case, namely the shrink of the nuclear ring and the precession of the inner ring which ensures the first separation and the later reconciliation.

The existence of neutral cases again reveals that the double ring is a potential phenomenon under our reasonable hypothesises rather than an accidental event.

7.3 Conclusion

We have drawn the conclusion that the inner ring origins from the primal gas residual, despite the deficiency of the qualitative analysis method. Clearly there are three key factors contributing to the double ring phenomenon. First, considerable primal gas is able to survive the exile of the bar torque, which is easy to reach in real nature since the non-asymmetric torque exerted on such a central place is certain to be relatively low as long as the mass of the non-asymmetric components is finite and gentle in the very centre. Second, appropriate periodic orbits exist inside the nuclear ring, which is as well easy to reach as long as it is not a critical case that the nuclear ring is just about to transform into x_1-type. Last but not the least, the isolation and inertia of the gas residual are the key to lead the gas into a self-evolution way. Inertia means that the inner ring is immune to all kinds of interference and stabilises at the specific location in a long while, which is the hardest to reach due to all kinds of interference in real nature like the star formation, the self-gravity of the gas and the magnetic field, which are all neglected in our simulation unfortunately. Even though the gas residual is able to be isolated and the inner ring exists on a moment in the nature, the later and long time of interference is bound to ruin it at all. Therefore the double ring phenomenon may not be as easy to be

(a) On 600 Myr (b) On 800 Myr (c) On 900 Myr

Figure 21: The case that the nuclear ring is considerably small.

(a) On 600 Myr (b) On 700 Myr

Figure 22: The case that the nuclear ring is considerably large.

Figure 23: An example of neutral case. The upper-left, upper-right, bottom-left, bottom-right are the snapshots on 400, 570, 800, $1000\,\mathrm{Myr}$ respectively.

found in real nature as in our numerical simulation.

In the addition, in order to improve our analysis and to confirm our argument, plenty of quantitative work is necessary to be done in the future like recording the momentum variation, determining the location of periodic orbits and tracking the gas flow.

References

[1] Athanassoula, E. 1992a, MNRAS, 259, 328

[2] Athanassoula, E. 1992b, MNRAS, 341, 1179A

[3] Kim, W.-T., Seo, W.-Y., Kim, Y. 2012b, ApJ, 758, 14

[4] Kim, W.-T., Seo, W.-Y., Stone, J. M., Yoon, D., Teuben, P. J. 2012a, ApJ, 747, 60

[5] Li, Z., Shen, J., Kim, W.-T. 2015, ApJ, 806, 150